CERN - European Organization for Nuclear Research

LCD-Note-2012-006

Physics performance for measurements of chargino and neutralino pair production at a 1.4 TeV CLIC collider

Philipp Roloff*

* *CERN, CH-1211 Geneva 23, Switzerland*

April 23, 2015

Abstract

A study of chargino and neutralino pair production at a CLIC collider operating at $\sqrt{s} = 1.4$ TeV is presented. Fully hadronic final states with four jets and missing transverse energy were considered. The analysis was performed using full detector simulation and including pileup from $\gamma\gamma \rightarrow$ hadrons interactions. Results for the masses and production cross sections of the chargino and the next-to-lightest neutralino are discussed.

Contents

1 Introduction

The Compact Linear Collider (CLIC) is a proposed electron-positron linear collider operated at centre-of-mass energies of up to 3 TeV [1]. The physics potential of CLIC is being studied using two detector concepts based on designs for the International Linear Collider (ILC) [2]. Several benchmark processes were investigated to address particular aspects of the detector performance goals for a CLIC collider operated at the highest possible energy of 3 TeV [3].

To achieve sufficient luminosities at very different centre-of-mass energies, a staged construction of CLIC is considered [4]. The physics implications of this staged construction were investigated studying additional benchmark processes. For this purpose, the production of several supersymmetric (SUSY) particles is investigated at $\sqrt{s} = 1.4$ TeV. One of these studies is described in this document.

The SUSY scenario assumed in this paper is described in more detail in [5]. In this model, the lightest chargino[1)], $\tilde{\chi}_1^+$, has a mass of 486.8 GeV, while the masses of the lightest and next-to-lightest neutralinos, $\tilde{\chi}_1^0$ and $\tilde{\chi}_2^0$, are given by 356.6 GeV and 486.7 GeV, respectively. The lightest neutral Higgs boson, h, has a mass of 117.8 GeV.

This SUSY model was chosen before the 126 GeV boson discovery at the LHC [6] was made. With small alterations a spectrum with the same qualitative features can be achieved where the lightest neutral Higgs boson has a mass of 126 GeV.

The following pair production processes for the lightest chargino and the next-to-lightest neutralino were investigated:

$$e^+e^- \to \tilde{\chi}_1^+\tilde{\chi}_1^- \to W^+\tilde{\chi}_1^0 W^-\tilde{\chi}_1^0 \text{ and} \tag{1}$$

$$e^+e^- \to \tilde{\chi}_2^0\tilde{\chi}_2^0 \to h(Z)\tilde{\chi}_1^0 h(Z)\tilde{\chi}_1^0, \tag{2}$$

where $BR(\tilde{\chi}_1^+ \to W^+\tilde{\chi}_1^0) = 99.8\%$, $BR(\tilde{\chi}_2^0 \to h\tilde{\chi}_1^0) = 94.6\%$ and $BR(\tilde{\chi}_2^0 \to Z\tilde{\chi}_1^0) = 5.1\%$. The h boson decays with a probablitiy of 63.7% into a beauty quark-antiquark pair, with a probability of 2.4% into a charm quark-antiquark pair, with a probability of 11.1% to $\tau^+\tau^-$ and with a probability of 8.0% into a gluon pair.

Hadronic decays of the W^+, h and Z bosons were considered and hence the investigated final state signature is given by four quarks and missing transverse energy. The measurement of chargino and neutralino pair production allows to assess the precicion which can be reached for the reconstruction of hadronically decaying gauge bosons in the presence of pileup from $\gamma\gamma \to$ hadrons interactions. The rather low energies of the reconstructed gauge or Higgs bosons represent a particular challenge for the background suppression and event reconstruction algorithms. The reconstruction at high energies was studied using a different SUSY model at $\sqrt{s} = 3$ TeV and is described elsewhere [7].

The analysis described in the following was performed assuming an integrated luminosity of 1.5 ab^{-1}, corresponding to about four years of data taking with 200 days of operation per year at 50% efficiency.

[1] Charge conjugation is implied throughout this paper.

2 The detector model

The study presented here was carried out using the CLIC_SiD detector model. CLIC_SiD is a general-purpose detector with a 4π coverage and is based on the SiD concept [8] developed for the ILC. It has been adapted [9] to meet the specific detector requirements at CLIC. A schematic overview of the CLIC_SiD detector is shown in Fig. 1.

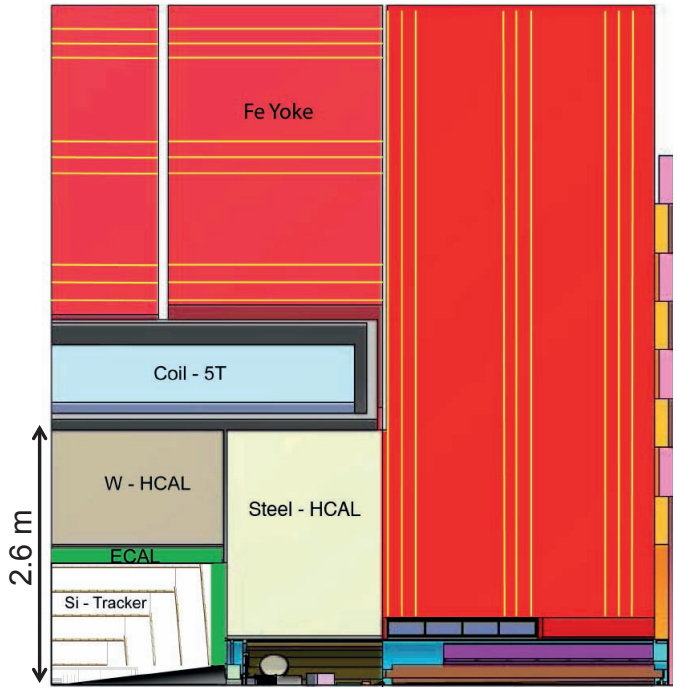

Figure 1: Longitudinal cross section of the top quadrant of CLIC_SiD [4].

A superconducting solenoid (Coil) with an inner radius of 2.7 m provides a central magnetic field of 5 T. The calorimeters are placed inside the coil and consist of a 30 layer tungsten–silicon electromagnetic calorimeter (ECAL) with 3.5×3.5 mm^2 segmentation, followed by a tungsten–scintillator hadronic calorimeter with 75 layers in the barrel region (W-HCAL) and a steel–scintillator hadronic calorimeter with 60 layers in the endcaps (Steel-HCAL). The read-out cell size in the hadronic calorimeters is 30×30 mm^2. The iron return yoke (Fe Yoke) outside of the coil is instrumented with nine double-RPC layers with 30×30 mm^2 read-out cells for muon identification.

The silicon-only tracking system (Si-Tracker) consists of five 20×20 µm^2 pixel layers followed by five strip layers with a read-out pitch of 50 µm and a length of 92 mm in the barrel region. The tracking system in the endcap consists of four stereo-strip disks with similar pitch and a stereo angle of 12°, complemented by seven pixelated disks in the vertex and far-forward region at lower radii with pixel sizes of 20×20 µm^2.

The forward region is instrumented with two compact electromagnetic calorimeters: LumiCal

with coverage down to 40 mrad and BeamCal with coverage down to 10 mrad.

The trigger-less readout accumulates hits over the full 156 ns bunch train. In the reconstruction it is assumed that all vertex and tracker hits are accompanied by a time-stamp in 10 ns bins, while the timestamping precision for calorimeter hits is 1 ns.

3 Monte Carlo samples

The physics events used for the study presented here were generated using the WHIZARD 1.95 [10] program. Initial and final state radiation (ISR and FSR) were enabled during the event generation. The treatment of ISR in WHIZARD is based on the LLA structure function [11]. Due to the intrinsic energy spread of the CLIC beams and the energy losses caused by beamstrahlung, not all the e^+e^- collisions at CLIC will take place at the nominal centre-of-mass energy. The resulting luminosity spectrum expected at CLIC was used during the event generation [12]. The effects of ISR and of the CLIC luminosity spectrum on the effective centre-of-mass energy for chargino and neutralino pair productions are shown in Fig. 2. Both effects result in long tails extending down to the production thresholds. Finally, the hadronisation of final state partons was simulated using PYTHIA [13].

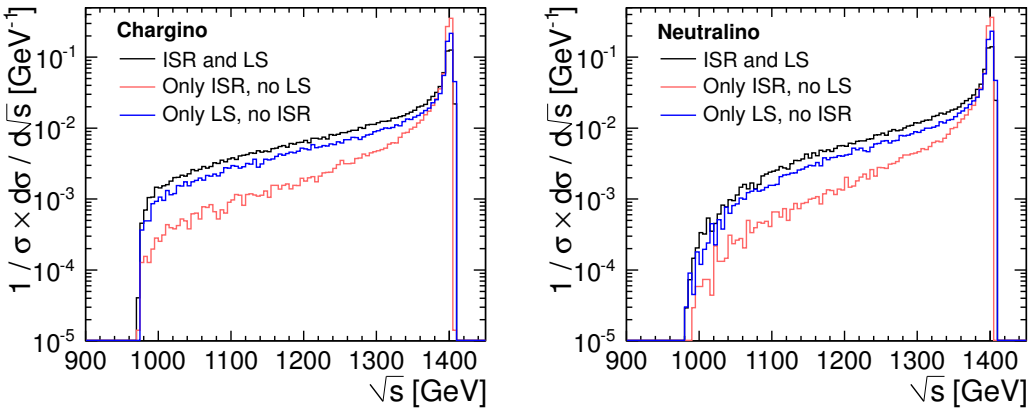

Figure 2: Normalised cross sections as functions of the effective centre-of-mass energy for chargino (left) and neutralino (right) pair production considering only ISR (red histograms) or only the luminosity spectrum (LS) at CLIC (blue histograms). The black histograms show the distributions obtained when both effects were used in the event generation.

An overview of all produced Monte Carlo (MC) samples is given in Tab. 1. Dedicated samples for the considered signals corresponding to large luminosities are available. Additionally, backgrounds from SUSY and Standard Model (SM) processes were used in the study presented in this paper.

Type	Final state	Cross section [fb]	Luminosity [ab^{-1}]	Referenced with
Signal	$\tilde{\chi}_1^+\tilde{\chi}_1^-$	15.3	9.7	Chargino
	$\tilde{\chi}_2^0\tilde{\chi}_2^0$	5.4	12.6	Neutralino
Background	$\tilde{\chi}_1^+\tilde{\chi}_1^-\nu\overline{\nu}$	0.36	63.3	SUSY
	$\tilde{\chi}_2^0\tilde{\chi}_2^0\nu\overline{\nu}$	0.36	35.0	
	$q\overline{q}h\nu\overline{\nu}$	2.2	7.4	Higgs
	$hh\nu\overline{\nu}$	0.23	80.0	
	$q(\overline{q})q(\overline{q})q(\overline{q})q(\overline{q})\nu\overline{\nu}$	24.7	8.7	SM

Table 1: Cross sections and integrated luminosities of the available Monte Carlo samples for chargino and neutralino pair production and for SUSY and Standard Model backgrounds. The charge conjugated modes are implied throughout this document.

All processes with at least four quarks or antiquarks and a neutrino-antineutrino pair in the final state were considered in the generation of the SM background sample. Other final states with four quarks or antiquarks, but without neutrinos or with charged leptons in the final state were not considered, because it is expected that these contributions can be easily rejected.

The final states $\tilde{\chi}_1^+\tilde{\chi}_2^-$ and $\tilde{\chi}_2^+\tilde{\chi}_2^-$ were not included in the analysis, because their cross sections were found to be negligible. The production of the heavier neutralinos, $\tilde{\chi}_3^0$ and $\tilde{\chi}_4^0$, is not accessible for a centre-of-mass energy of 1.4 TeV.

4 Event simulation and reconstruction

The generated events were passed through the detector simulation program SLIC [14] which is based on the Geant4 [15] package. The CLIC_SiD detector geometry as described above was used.

At a 1.4 TeV CLIC collider, 1.3 $\gamma\gamma \to$ hadrons events with a $\gamma\gamma$ centre-of-mass energy greater than 2 GeV are produced on average per bunch crossing. The bunch spacing of only 0.5 ns leads to pileup in the subdetectors of CLIC_SiD which integrate over multiple bunch crossings.

To take into account the impact of pileup on the measurement described in the following, each physics event was overlaid with a sample of $\gamma\gamma \to$ hadrons events corresponding to 60 bunch crossings [18]. The $\gamma\gamma \to$ hadrons events were passed through the same simulation of the CLIC_SiD detector based on Geant4 as the physics events. The choice of 60 bunch crossings represents a compromise between a realistic description of the experimental conditions at CLIC and computing constraints.

The event reconstruction was performed in a window of 10 ns around the time of the physics event for all subdetectors, except for the W-HCAL where a window of 100 ns was assumed. The assumed precision of 1 ns to measure hit times in the calorimeters leads to sub-ns precision for cluster times given by the truncated mean of the corresponding hit times.

Calorimeter and tracking information were combined in the particle flow approach to recon-

struct particles. For this purpose, an improved version [16] of the PandoraPFA [17] algorithm was used. The production time of a reconstructed particle was obtained by correcting the cluster time for its flight time through the magnetic field. This production time of each reconstructed particle was required to be consistent with the time of the physics event. The allowed time intervals depended on the particle type, transverse momentum and polar angle [19]. As an example, these cuts reduced the mean number of particles in the reconstruction window by a factor 5.5 and their mean total momentum by a factor 2.7 for chargino pair production events.

5 Reconstruction of W^+ and Higgs bosons

The steps to reconstruct events with four jets are described in this section. First, events with at least one identified electron or muon with $p_T > 20$ GeV were rejected to remove leptonic W^+ decays. Reconstructed particles were used as input to the jet clustering. The k_t algorithm [20] as implemented in FastJet [21] in its exclusive mode with $R = 1.0$ and using the E recombination scheme was chosen. The clustering was stopped when four jets were found. To reject decays of W^+, Z or Higgs bosons to τ leptons, all jets were required to contain at least four PFOs. Events were rejected if at least one of the jets was outside the kinematic region defined by: $E^{\text{jet}} > 5$ GeV and $|\cos\theta^{\text{jet}}| < 0.975$.

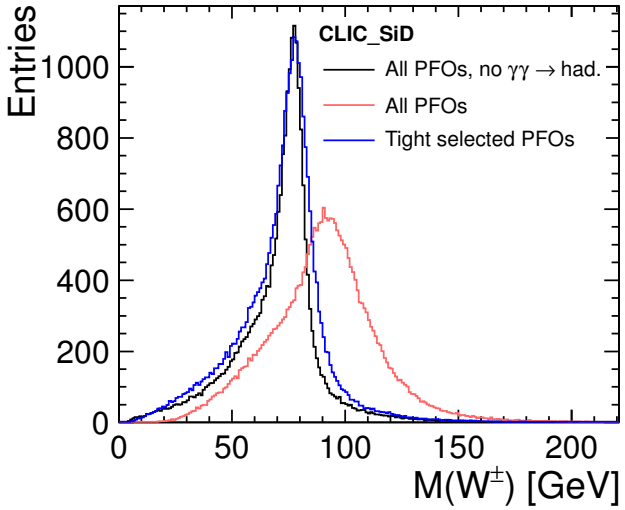

Figure 3: Reconstructed mass of W^+ candidates in $e^+e^- \to \tilde{\chi}_1^+\tilde{\chi}_1^-$ events without overlay of $\gamma\gamma \to$ hadrons (black histogram), with overlay of $\gamma\gamma \to$ hadrons (red histograms) and using selected PFOs (blue histogram).

Boson candidates were formed from jet pairs by minimising:

$$(M_{jj,1} - M_{W^+,h})^2 + (M_{jj,2} - M_{W^+,h})^2, \tag{3}$$

where $M_{jj,1}$ and $M_{jj,2}$ are the masses of the two reconstructed jet pairs and $M_{W^+,h}$ was set to the world average of the W^+ boson mass to reconstruct $\tilde{\chi}_1^+$and to the assumed Higgs boson mass in the event generation to reconstruct $\tilde{\chi}_2^0$.

As an example, the invariant mass of reconstructed W^+ bosons is shown in Fig. 3. The distributions with and without overlay of pileup from $\gamma\gamma \to$ hadrons interactions are compared. The peak is widened and shifted to a larger mass due to the $\gamma\gamma \to$ hadrons events. When combined timing and transverse momentum cuts as discussed in Sec. 4 are applied, the peak is located at the nominal W^+ mass and only somewhat wider compared to the original distribution without overlay of $\gamma\gamma \to$ hadrons events.

6 Event selection

The selection of $\tilde{\chi}_1^+$and $\tilde{\chi}_2^0$ pair production events was performed in two steps. First, a cut-based preselection was applied. The remaining background events were suppressed further using boosted decision trees as implemented in TMVA [22] in a second step. These two steps are described in the following two subsections.

6.1 Preselection cuts

To restrict the training of the boosted decision trees to the region where the signal purities are high, the following preselection cuts were applied:

- 40 GeV $< M_{\mathrm{jj},1} <$ 160 GeV and 40 GeV $< M_{\mathrm{jj},2} <$ 160 GeV;
- $|\cos\theta^{\mathrm{jj},1}| < 0.95$ and $|\cos\theta^{\mathrm{jj},2}| < 0.95$, where $\theta^{\mathrm{jj},1}$ and $\theta^{\mathrm{jj},2}$ are the polar angles of the two jet pairs;
- $|\cos\theta^{\mathrm{miss}}| < 0.95$, where θ^{miss} is the polar angle of the missing momentum;
- $p_T^{\mathrm{miss}} <$ 250 GeV, where p_T^{miss} is the missing transverse momentum;
- $E^{\mathrm{vis}} <$ 600 GeV, where E^{vis} is the total visible energy of the event.

The energy distributions of the reconstructed W^+ and Higgs candidates after these cuts were imposed are shown in Fig. 4.

6.2 Event selection using boosted decision trees

To train the boosted decision trees, 20% of the available events for each process were used. These events were not considered in the analysis to measure masses or cross sections. The boosted decision trees were trained using 17 variables describing the event topology and describing kinematic quantities of the reconstructed W^+ or Higgs candidates:

- missing transverse momentum;
- thrust of the event;

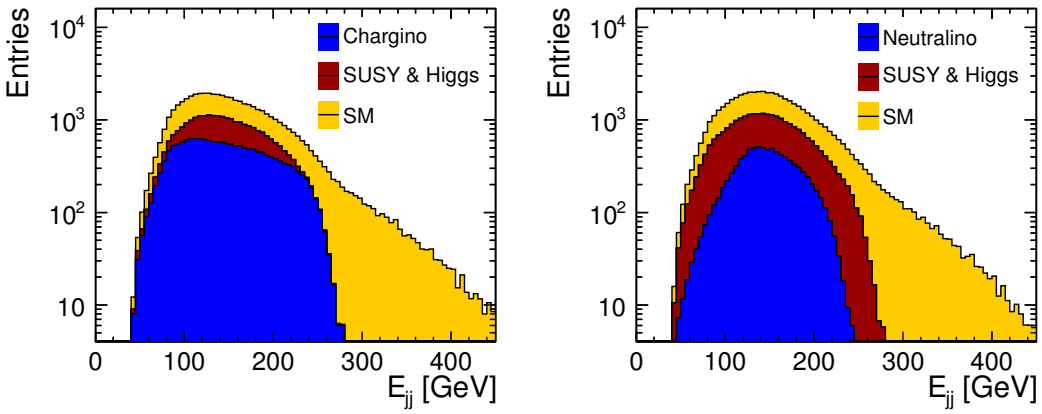

Figure 4: Energy spectra of W^+ candidates in chargino signal and background events (left) and of Higgs candidates in neutralino signal and background events (right) after the preselection cuts were applied. The different contributions are shown by stacked histograms. All contributions were scaled to an integrated luminosity of 1.5 ab^{-1}.

- oblateness of the event;
- acoplanarity defined as the angular distance between the two W^+ or Higgs candidates in the plane perpendicular to the beam axis;
- $\cos\theta^{\mathrm{jj},1}$ and $\cos\theta^{\mathrm{jj},2}$ as defined in Sec. 6.1;
- angle between the two W^+ or Higgs candidates;
- θ^{miss} as defined in Sec. 6.1;
- invariant masses, $M_{\mathrm{jj},1}$ and $M_{\mathrm{jj},2}$, of each W^+ or Higgs candidate, and of the sum of both;
- weighted charge of each jet pair, $\frac{\sum_i q_i \cdot (p_i^{\mathrm{PFO}})^\kappa}{\sum_i (p_i^{\mathrm{PFO}})^\kappa}$, where the sum runs over all PFOs, p_i^{PFO} is the momentum of the i^{th} PFO and $\kappa = 1.8$;
- number of reconstructed particles in each jet pair;
- total visible energy in the event;
- number of reconstructed particles in the event.

None of these variables is strongly correlated to the energies of the W^+ and Higgs candidates which are used to measure masses and cross sections. The outputs of the boosted decision trees for signal and background events are shown in Fig. 5. As expected, the signals tend to higher values than the backgrounds.

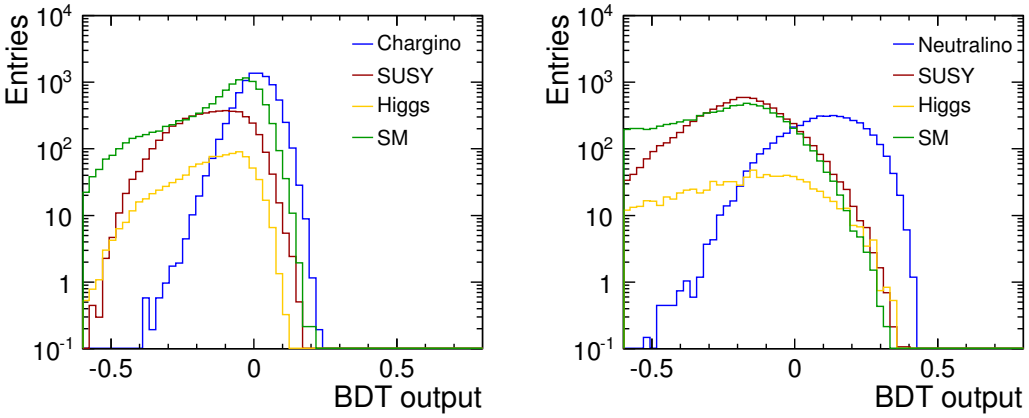

Figure 5: Outputs of the boosted decision trees for the chargino (left) and neutralino (right) selections. The signals (blue histograms) are compared to the different background contributions.

Events were selected using cuts on the outputs of the boosted decision trees. The cut values were chosen maximising the significance defined as:

$$S = \frac{S}{\sqrt{S+B}}, \tag{4}$$

where S is the number of signal events and B is the number of background events for a given cut. The cut values of -0.0677 and 0.0158 were used for the chargino and neutralino selections, respectively. The resulting energy spectra of the reconstructed W^+ and Higgs candidates are shown in Fig. 6. These energy distributions were used to measure cross sections and masses as described in the next section.

An overview of the fraction of chargino and neutralino pair production events passing different steps of the event reconstruction and selection chain as described above is shown in Tab. 2. The percentages were calculated relative to the total number of $\tilde{\chi}_1^+\tilde{\chi}_1^-$ and $\tilde{\chi}_2^0\tilde{\chi}_2^0$ events irrespective of the decays of the W^+ and Higgs bosons. The total efficiency of the complete analysis chain is 33% for chargino pairs and 41% for neutralino pairs. It is expected that the reconstruction efficiency for chargino pair production events is smaller than for neutralino pair production events due to the larger probability for the W^+ bosons to decay into leptons compared to the Higgs bosons.

7 Cross section and mass extraction

The pair production cross sections were determined using:

$$\sigma = \frac{(N_{\text{data}} - N_{\text{bkg}})}{2 \cdot \varepsilon \cdot \mathscr{L}},$$

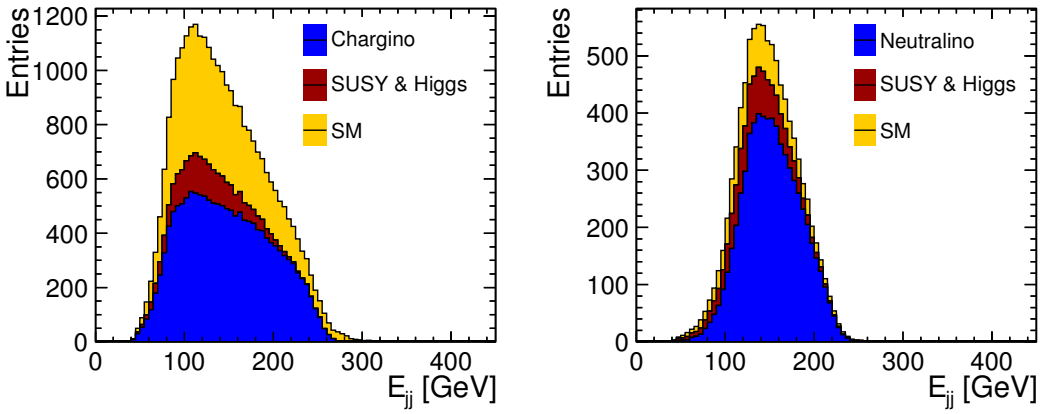

Figure 6: Energy spectra of W^+ candidates in chargino signal and background events (left) and of Higgs candidates in neutralino signal and background events (right) after the full event selection was applied. The different contributions are shown by stacked histograms. All contributions were scaled to an integrated luminosity of 1.5 ab^{-1}.

	$\tilde{\chi}_1^+\tilde{\chi}_1^-$	$\tilde{\chi}_2^0\tilde{\chi}_2^0$
After event reconstruction	48%	66%
After preselection cuts	37%	55%
After cut on BDT output	33%	41%

Table 2: Fraction of chargino and neutralino pair production events after different steps of the event reconstruction and selection chain.

where N_{data} is the total number of reconstructed boson candidates, N_{bkg} is the number of reconstructed boson candidates in the background events, ε is the overall signal efficiency and $\mathscr{L} = 1.5$ ab^{-1} is the integrated luminosity. The following cross section for chargino pair production was obtained:

$$\sigma(e^+e^- \to \tilde{\chi}_1^+\tilde{\chi}_1^-) = 15.32 \pm 0.17 \text{ fb}.$$

The corresponding result for neutralino pair production is given by:

$$\sigma(e^+e^- \to \tilde{\chi}_2^0\tilde{\chi}_2^0) = 5.40 \pm 0.08 \text{ fb}.$$

Both values are in excellent agreement with the cross sections assumed during the event generation (see Tab. 1).

The energy distributions of reconstructed Higgs and W^+ candidates are sensitive to the masses of the $\tilde{\chi}_1^+$and $\tilde{\chi}_2^0$ particles. To determine the masses of the investigated SUSY particles, the

template method was used. Signal Monte Carlo samples for different mass hypotheses were generated and passed through the full detector simulation. The masses of the $\tilde{\chi}_1^{\pm}$ and $\tilde{\chi}_2^0$ particles were varied separately keeping the masses of all other SUSY particles at their default values. For each SUSY particle, six templates with luminosities of about 10 ab^{-1} were used. Pileup from $\gamma\gamma \to$ hadrons was overlaid during the production of the templates as described in Sec. 4. In Fig. 7 the dependencies of the reconstructed energy distributions on the chargino and neutralino masses is illustrated.

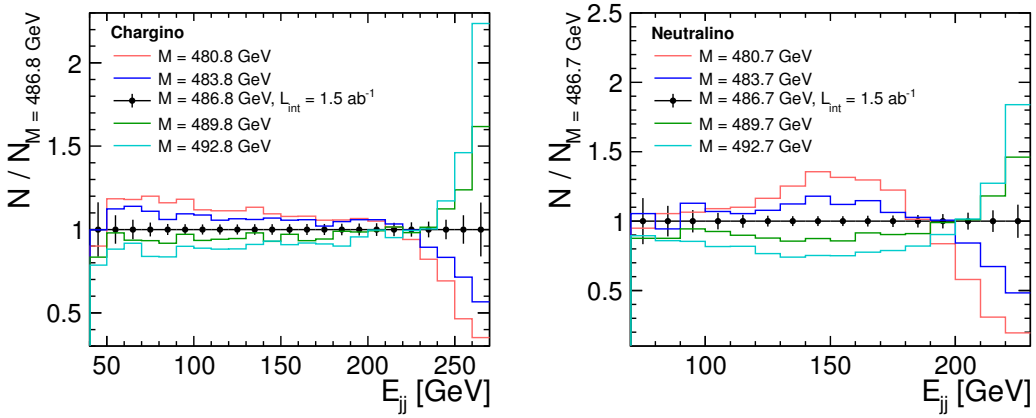

Figure 7: Ratios of the reconstructed energy distributions of W^+ (left) or Higgs (right) candidates for templates generated assuming different values of the $\tilde{\chi}_1^+$or $\tilde{\chi}_2^0$ masses to the energy distributions obtained using the default mass values. The error bars show the statistical uncertainties assuming an integrated luminosity of 1.5 ab^{-1}.

Two-dimensional fits were performed simultaneously to the mass and production cross section for a given particle to account for the correlation between both quantities. The obtained precisions for the pair production cross sections are in good agreement with the independent cross section extraction described above.

The toy MC method was used to estimate the statistical uncertainties of the measured masses. For this purpose, the data points in the measured boson energy distributions were smeared using a Gaussian distribution of width $\sqrt{n_{\text{data},i}}$, where $n_{\text{data},i}$ is the number of entries in a given bin. This step was repeated 5000 times and the optimal values were extracted for each iteration. The standard deviations of these optimal values represent the statistical uncertainties of the measured masses.

The following masses were obtained assuming an integrated luminosity of 1.5 ab^{-1}:

$$M(\tilde{\chi}_1^+) = 487.4 \pm 0.8 \text{ GeV and } M(\tilde{\chi}_2^0) = 487.9 \pm 0.5 \text{ GeV},$$

which are in reasonable agreement with the values assumed during the event generation.

8 Systematic uncertainties

A detailed evaluation of the systematic uncertainties expected to affect the measurement of gaugino pair production using hadronic final states is not possible at this moment, because many relevant details on the detector implementation are still unknown. Additionally, the size of some systematic errors will depend on other measurements. Hence the impact of a few effects, which are expected to be most relevant, are illustrated in the following.

Uncertainty of $M(\tilde{\chi}_1^0)$

The energy distributions of reconstructed W^+ or Higgs candidates are also sensitive to the mass of the lightest neutralino, $M(\tilde{\chi}_1^0)$. It was found that three parameter fits to extract $M(\tilde{\chi}_1^0)$ simultaneously with $M(\tilde{\chi}_1^+)$ or $M(\tilde{\chi}_2^0)$ and the pair production cross sections have no localised minima. Hence an uncertainty on $M(\tilde{\chi}_1^0)$ of 1 GeV was assumed. It is expected that this precision can be achieved using slepton production [23]. The uncertainty on $M(\tilde{\chi}_1^0)$ was propagated to $M(\tilde{\chi}_1^+)$ and $M(\tilde{\chi}_2^0)$. The resulting uncertainties on $M(\tilde{\chi}_1^+)$ and $M(\tilde{\chi}_2^0)$ are ± 1.4 GeV and ± 1.3 GeV, respectively.

Jet energy scale

A precise knowledge of the absolute jet energy scale is crucial for mass measurements in hadronic final states. To demonstrate this effect, the jet energies for the fitted distributions were scaled by $\pm 1\%$ while the templates were kept unchanged. This variation resulted in a $^{+2.8}_{-3.4}$ GeV shift on $M(\tilde{\chi}_1^+)$ and a $^{+1.1}_{-1.4}$ GeV shift on $M(\tilde{\chi}_2^0)$. It is expected that the jet energy scale will be understood to a better accuracy at CLIC.

Luminosity spectrum

To illustrate the effect of the uncertainty of the luminosity spectrum measurement, two variants of the luminosity spectrum were created "ad-hoc", in an attempt to mimic a change in beam conditions at the IP. In the first variant, for each beam 1% of the events were removed from the high energy peaks of the distributions and randomly distributed in the tails. As a second variation, the same number of events was moved from the tails of the distributions to the peaks.

The template fits were repeated with these distorted luminosity spectra used for the measured signal events while the templates were kept unchanged. This procedure simulates the effect of a limited understanding of the luminosity spectrum in measured data. The variations lead to changes in the extracted cross sections which are about the same size as the statistical uncertainties. The impact on the mass measurements was found to be negligible.

9 Summary and conclusions

The signals from $\tilde{\chi}_1^+$ and $\tilde{\chi}_2^0$ pair production were extracted from fully hadronic final states with four jets and missing transverse energy at $\sqrt{s} = 1.4$ TeV. The study was performed using full detector simulation and considering pileup from $\gamma\gamma \to$ hadrons. Backgrounds from SUSY and

SM processes were included. Assuming an integrated luminosity of 1.5 fb^{-1}, the chargino and neutralino pair production cross sections were extracted with statistical precisions of about 1.3%, while the masses of the $\tilde{\chi}_1^+$ and $\tilde{\chi}_2^0$ particles were determined with typical statistical accuracies of less than 1 GeV. The precisions of the masses degrade to about 1.5 GeV if an uncertainty of 1 GeV on $M(\tilde{\chi}_1^0)$ is assumed.

These results demonstrate that precise measurements in multi-jet final states are possible at a 1.4 TeV CLIC collider despite challenging beam-related backgrounds. This is important, because the reconstruction of hadronic gauge boson and Higgs decays is a crucial aspect of many searches for physics beyond the Standard Model at a high-energy e^+e^- collider. The CLIC_SiD detector concept is well suited for these measurements.

Chargino and neutralino pair production as discussed in this paper is an example that e^+e^- colliders like CLIC are well suited to study heavy weakly interacting states. Such measurements are far more challenging at hadron colliders due to the large QCD backgrounds.

References

[1] M. Aicheler (Ed.) et al., *A Multi-TeV Linear Collider based on CLIC Technology - CLIC Conceptual Design Report*, CERN-2012-007 (2012).

[2] N. Phinney, N. Toge and N. Walker (Eds.), *International Linear Collider Reference Design Report - Volume 3: Accelerator*, arXiv:0712.2361 (2007).

[3] L. Linssen (Ed.) et al., *Physics and Detectors at CLIC - CLIC Conceptual Design Report*, CERN-2012-003 (2012).

[4] P. Lebrun (Ed.) et al., *The CLIC Programme: Towards a staged e^+e^- Linear Collider exploring the Terascale - CLIC Conceptual Design Report*, CERN-2012-005 (2012).

[5] B. Allanach et al., *The physics benchmark processes for the detector performance studies of the CLIC CDR Volume 3*, LCD-Note-2012-003 (2012).

[6] G. Aad et al. [Atlas Coll.], *Observation of a new particle in the search for the standard model higgs boson with the ATLAS detector at the LHC*, Phys. Lett. **B 716**, 1 (2012);
S. Chatrchyan et al. [CMS Coll.], *Observation of a new boson at a mass of 125 GeV with the CMS experiment at the LHC*, Phys. Lett. **B 716**, 30 (2012).

[7] T. Barklow, A. Münnich and P. Roloff, *Measurement of chargino and neutralino pair production at CLIC*, LCD-Note-2011-037 (2011);
P. Roloff, T. Barklow and A. Münnich, *Measurement of Chargino and Neutralino Production at CLIC*, Proceedings of LCWS11, arXiv:1202.5489 (2012).

[8] H. Aihara, P. Burrows and M. Oreglia (Eds.), *SiD Letter of Intent*, arXiv:0911.0006 (2009).

[9] C. Grefe and A. Münnich, *The CLIC_SiD_CDR Detector Model for the CLIC CDR Monte Carlo Mass Production*, LCD-Note-2011-009 (2011).

[10] W. Kilian, T. Ohl and J. Reuter, *WHIZARD: Simulating Multi-Particle Processes at LHC and ILC*, arXiv:0708.4233 (2007);
M. Moretti et al., *O'Mega: An Optimizing Matrix Element Generator*, LC-TOOL-2001-040, also arXiv:hep-ph/0102195 (2001).

[11] M. Skrzypek and S. Jadach, *Exact and approximate solutions for the electron nonsinglet structure function in QED*, Z. Phys. **C 49**, 577 (1991).

[12] B. Dalena, J. Esberg and D. Schulte, *Beam-induced backgrounds in the CLIC 3 TeV CM energy interaction region*, Proceedings of LCWS11, arXiv:1202.0563 (2012).

[13] T. Sjörstrand, S. Mrenna and P. Skands, *PYTHIA 6.4 physics and manual*, JHEP **05**, 026 (2006).

[14] N. Graf and J. McCormick, *Simulator For The Linear Collider (SLIC): A Tool For ILC Detector Simulations*, AIP Conf. Proc. **867**, 503 (2006).

[15] S. Agostinelli et al., *GEANT4 - a simulation toolkit*, Nucl. Instr. Meth. **A 506**, 250 (2003);
J. Allison et al., *Geant4 Developments and Applications*, IEEE Trans. Nucl. Sci. **53**, 270 (2006).

[16] J. Marshall and M.A. Thomson, *Redesign of the Pandora Particle Flow algorithm*, Report at IWLC2010 (2010).

[17] M.A. Thomson, *Particle Flow Calorimetry and the PandoraPFA Algorithm*, Nucl. Inst. Meth. **A 611**, 25 (2009).

[18] C. Grefe, *OverlayDriver - an Event Mixing Tool for org.lcsim*, LCD-Note-2011-032 (2011).

[19] J. Marshall, A. Münnich and M.A. Thomson, *Particle Flow Performance at CLIC*, LCD-Note-2011-028 (2011).

[20] S. Catani et al., *Longitudinally-invariant $k_\perp$-clustering algorithms for hadron-hadron collisions*, Nucl. Phys. **B 406**, 187 (1993);
S.D. Ellis and D.E. Soper, *Successive combination jet algorithm for hadron collisions*, Phys. Rev. **D 48**, 3160 (1993).

[21] M. Cacciari, G.P. Salam, *Dispelling the N^3 myth for the k_t jet-finder*, Phys. Lett. **B 641**, 57 (2006);
M. Cacciari, G.P. Salam and G. Soyez, *FastJet user manual*, arXiv:1111.6097 (2011).

[22] A. Hoecker et al., *TMVA: Toolkit for Multivariate Data Analysis*, PoS ACAT, 40 (2007).

[23] M. Battaglia et al., *Physics performances for Scalar Electron, Scalar Muon and Scalar Neutrino searches at $\sqrt{s} = 3$ TeV and* 1.4 *TeV at CLIC*, LCD-Note-2012-012 (2012).